

# A 3-D Wideband Multi-Confocal Ellipsoid Model for Wireless MIMO Communication Channels

Lu Bai<sup>1</sup>, Cheng-Xiang Wang<sup>2</sup>, Shangbin Wu<sup>3</sup>, Haowen Wang<sup>4</sup>, Yang Yang<sup>4</sup>

<sup>1</sup>School of Information Science and Engineering, Shandong University, Shandong 250100, China.

<sup>2</sup>School of Engineering and Physical Sciences, Heriot-Watt University, Edinburgh, EH14 4AS, UK.

<sup>3</sup>Samsung R&D Institute UK, Staines-upon-Thames, TW18 4QE, UK.

<sup>4</sup>Shanghai Research Center for Wireless Communications, Shanghai, 200000, China.

Email: bailusdu@126.com, cheng-xiang.wang@hw.ac.uk, shangbin.wu@samsung.com, {haowen.wang, yang.yang}@wico.sh

**Abstract**—This paper first proposes a novel three dimensional (3-D) wideband multi-confocal ellipsoid model for wireless multiple-input multiple-output (MIMO) communication channels. The proposed 3-D geometry-based stochastic model (GBSM) describes the channel in both the azimuth direction and elevation direction, including delay, Doppler frequency, angle of departure (AoD), and angle of arrive (AoA). It can be shown that the ellipsoid model can capture the effect of the clusters more accurately than the previous elliptic-cylinder model. Using the proposed theoretical model as the reference model, the corresponding simulation model is also derived. Numerical results demonstrate that their statistical properties can match well.

**Keywords** – Wideband multi-confocal ellipsoid model, MIMO, GBSM, 3-D model, statistical properties.

## I. INTRODUCTION

To improve the reliability and efficiency of wireless communication systems, MIMO techniques have been widely used. One of the most important challenges for practical MIMO system design is to get an accurate, general, and easy-to-use model to describe the underlying realistic propagation channels [1].

MIMO stochastic channel models can be categorized as correlation-based stochastic models (CBSMs) and GBSMs. CBSMs include the identically and independently distributed (i.i.d.) channel model, Kronecker-based stochastic model (KBSM), Weichselberger model [2], and virtual channel representation (VCR) [3]. The i.i.d. channel model is over-simplified to analyze MIMO technologies precisely. The KBSMs in [4]–[7] neglected the dependency between the transmitter (Tx) spatial correlation matrix and receiver (Rx) spatial correlation matrix, while the Weichselberger model in [2] and the VCR in [3] took mutual coupling effects between the Tx and Rx into consideration. The differences among these three models were discussed in detail in [2] and [8]. GBSMs can be divided into pure-GBSMs and semi-GBSMs. In pure-GBSM, scatterers are assumed to be located on an exact geometry, such as a two-dimensional (2-D) one-ring model in [9], two-ring models in [10] and [11], an ellipse model in [12], combined two-ring and ellipse models in [13] and [14], and a 3-D elliptic-cylinder model in [15]. The standard models such as the COST 2100 model in [16], spatial channel model (SCM), SCM-Extend

(SCM-E) model, WINNER models in [17] (WINNER I/II in 2-D models and WINNER+ in 3-D models), and IMT-Advanced (IMT-A) model in [18], are all semi-GBSMs whose scatterers are described by certain distributions. There are also some user-defined parameters such as delay, AoA, AoD, and Doppler frequency.

Compared to 2-D models, 3-D models are able to capture channel characteristics in the elevation direction. Although the 3-D elliptic-cylinder model in [15] claimed that it considered elevation angles, scatterers located on the elliptic-cylinder do not have the same delays. This violates the advantage of elliptic models for wideband channels. To overcome this problem, in this paper a novel 3-D theoretical wideband multi-confocal ellipsoid MIMO channel model is first proposed which is capable of modeling clusters with identical delays in the same ellipsoid while different ellipsoids represent different delays of clusters. Also, elevation angles and rotations of antenna arrays are considered. The simulation model of the proposed theoretical reference model is also derived.

The remainder of the paper is as follows. Section II describes the 3-D theoretical wideband multi-confocal ellipsoid model. The statistical properties of the proposed reference model are derived in Section III. Section IV presents the corresponding simulation model. The results and analysis are given in Section V. Last, conclusions are drawn in Section VI.

## II. THEORETICAL REFERENCE MODEL

In the theoretical reference model shown in Fig.1, each ellipsoid is the rotation of an ellipse with respect to the  $y$  axis. The Tx and Rx are equipped with uniform linear arrays (ULAs) with  $M_T$  and  $M_R$  omnidirectional antennas, respectively. The central points of ULAs are located at the focal points of the confocal ellipsoids with a distance of  $2f$ . The antenna spacings of the Tx and Rx are  $\delta_T$  and  $\delta_R$ , respectively. Note that  $\mathbf{A}_k^T$  represents the vector of the  $k$ th receive antenna and  $\mathbf{A}_l^R$  represents the vector of the  $l$ th transmit antenna.

The antennas have different coordinates in the global coordinate system (GCS) and local coordinate system (LCS). The GCS is defined for the scattering environment. The antenna arrays of Tx and Rx can be defined in the LCS.

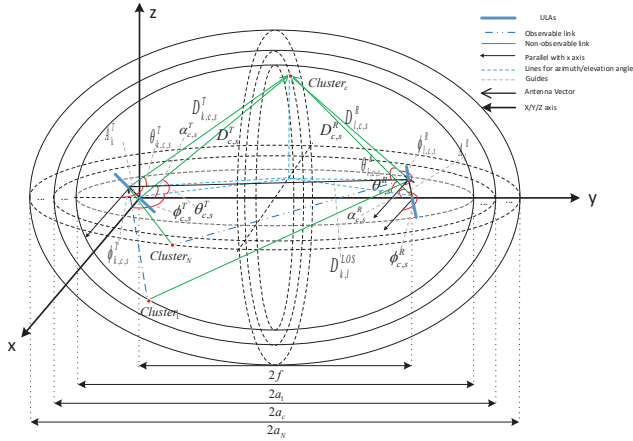


Fig. 1: A 3-D wideband multi-confocal ellipsoid model for wireless MIMO communication channels.

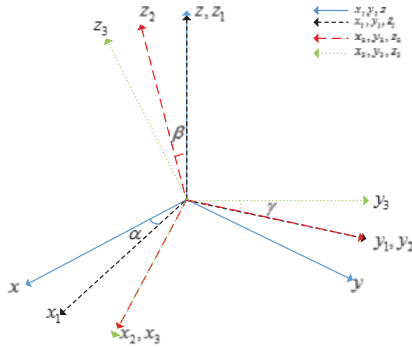


Fig. 2: Orienting the LCS with respect to the GCS by a sequence of 3 rotations:  $\alpha, \beta, \gamma$ .

In the LCS, the antenna vector in the Tx is  $\mathbf{A}'_k{}^T = [x'_k{}^T, y'_k{}^T, z'_k{}^T]^T$ , while the antenna vector in the Rx is  $\mathbf{A}'_l{}^R = [x'_l{}^R, y'_l{}^R, z'_l{}^R]^T$ , where

$$x'_k{}^T = \begin{cases} -\frac{m-2k+1}{2}\delta_T, & k < \frac{m+1}{2}, \\ \frac{m-2k+1}{2}\delta_T, & k \geq \frac{m+1}{2} \end{cases} \quad (1)$$

$$y'_k{}^T = 0 \quad (2)$$

$$z'_k{}^T = 0 \quad (3)$$

$$x'_l{}^R = \begin{cases} -\frac{p-2l+1}{2}\delta_R, & l < \frac{p+1}{2}, \\ \frac{p-2l+1}{2}\delta_R, & l \geq \frac{p+1}{2} \end{cases} \quad (4)$$

$$y'_l{}^R = 0 \quad (5)$$

$$z'_l{}^R = 0. \quad (6)$$

The placement of the antenna arrays within the GCS is defined by the transformation between the GCS and the LCS. The orientation of the array with respect to the GCS is defined in general by a sequence of rotations in [19]. In Fig. 2, we consider an arbitrary 3-D rotation of the LCS with respect to the GCS given by the angles  $\alpha, \beta$ , and  $\gamma$ . The  $x_1, y_1, z_1$  axes are the original  $x, y, z$  axes after the first rotation of  $\alpha$  with respect to  $z$ . Similarly, the  $x_2, y_2, z_2$  axes are obtained from the  $x_1, y_1, z_1$  axes after the second rotation of  $\beta$  with respect to  $y$ . Finally, the  $x_3, y_3, z_3$  axes are the  $x_2, y_2, z_2$  axes after the third rotation of  $\gamma$  with respect to  $x$ . The orientation of the  $x, y, z$  axes after all three rotations can be denoted as  $x_3, y_3, z_3$  which represent the final orientations of the LCS. In order to establish the equations for transformation of the coordinate system and the antenna field patterns between the GCS and LCS, it is necessary to determine the composite rotation matrix that describes the transformation of the points  $x, y, z$  in the GCS into the points  $x_3, y_3, z_3$  (denoted as  $x', y', z'$ , respectively) in the LCS. Note that

$$\mathbf{A}'_k{}^T = \mathbf{R}\mathbf{A}'_k{}^T \quad (7)$$

$$\mathbf{A}'_l{}^R = \mathbf{R}\mathbf{A}'_l{}^R \quad (8)$$

$$\mathbf{R} = \mathbf{R}_Z(\alpha)\mathbf{R}_Y(\beta)\mathbf{R}_X(\gamma) = \begin{pmatrix} +\cos\alpha & -\sin\alpha & 0 \\ +\sin\alpha & -\cos\alpha & 0 \\ 0 & 0 & 1 \end{pmatrix} \begin{pmatrix} +\cos\beta & 0 & -\sin\beta \\ 0 & 1 & 0 \\ -\sin\beta & 0 & +\cos\beta \end{pmatrix} \begin{pmatrix} 1 & 0 & 0 \\ 0 & +\cos\gamma & -\sin\gamma \\ 0 & +\sin\gamma & +\cos\gamma \end{pmatrix}. \quad (9)$$

The  $c$ th cluster of scatters is on the  $c$ th ellipsoid with major axis  $2a_c$ ,  $\mathbf{v}$  denotes the vector of movement of the receiver, the maximum Doppler frequency and carrier wavelength are denoted as  $f_{\max}$  and  $\lambda$ , respectively. Also, let  $N$  denote the total number of clusters which are observable to transmit and receive antennas.

The definitions of the key parameters for the proposed 3-D theoretical MIMO channel model are given Table I. The wideband MIMO channel can be characterized by an  $M_R \times M_T$  ( $q \times m$ ) complex matrix [20] [21]:

$$\mathbf{H}(t, \tau) = \begin{bmatrix} h_{11} & h_{12} & \cdots & h_{1m} \\ h_{21} & h_{22} & \cdots & h_{2m} \\ \vdots & \vdots & \ddots & \vdots \\ h_{q1} & h_{q2} & \cdots & h_{qm} \end{bmatrix} \quad (10)$$

where  $k = 1, 2, \dots, m$  and  $l = 1, 2, \dots, q$ . Next, let us assume that the initial phase of the signal at the Tx is  $\phi_0$ , LOS Rician factor is  $K$ , and the LOS component only exists for the first ellipsoid. Additionally, let us assume that the mean power of the  $c$ th cluster is  $P_c$  and there are  $S$  rays within one cluster. Note that  $\alpha_{c,s}^T$  is the AoD between  $D_{c,s}^T$  and  $y$  axis

TABLE I: Summary of key parameter definitions.

Symbol	Definition
$\delta_T(\delta_R)$	antenna spacing of transmit (receive) antenna array
$M_T(M_R)$	number of transmit (receive) antennas
$\mathbf{A}_k^T(\mathbf{A}_l^R)$	the $k(l)$ th antenna of transmit(receive) antenna array
$\alpha, \beta, \gamma$	rotary angle about $z, y, x$ .
$2f$	distance between the transmitter and receiver (focal length)
$\mathbf{v}$	velocity vector of the receiver antenna array
$\mathbf{v}_c$	velocity vector of the $c$ th cluster
$a_c$	semi-major axis of the $n$ th ellipsoid
$f_{\max}, \lambda$	maximum Doppler frequency and carrier wavelength
$\mathbf{D}_{l,k}^{\text{LOS}}$	vector of LOS path from the $k$ th antenna of transmitter to the $l$ th antenna of receiver
$\mathbf{D}_{l,0}^{\text{LOS}}$	vector of LOS path from the central point of transmitter to the $l$ th antenna of receiver
$\mathbf{D}_{k,c,s}^T$	vector from the $k$ th antenna of transmitter to the $c$ th cluster via the $s$ th ray within the cluster
$\mathbf{D}_{c,s}^T$	vector from transmitter to the $c$ th cluster via the $s$ th ray
$\mathbf{D}_{l,c,s}^R$	vector from the $c$ th cluster to the $l$ th antenna of receiver via the $s$ th ray within the cluster
$\mathbf{D}_{c,s}^R$	vector from $c$ th cluster to receiver via the $s$ th ray
$f_{l,k}^{\text{LOS}}$	doppler frequency of LOS path from the $k$ th antenna of transmitter to the $l$ th antenna of receiver
$f_{c,s}$	doppler frequency of the $c$ th cluster via the $s$ th ray
$\phi_{l,k}^{\text{LOS}}$	phase of LOS path from the $k$ th antenna of transmitter to the $l$ th antenna of receiver
$\phi_0$	initial phase of the signal at the transmitter
$P_c$	the mean power of the $c$ th cluster
$K/S$	LOS Rician factor and number of rays within one cluster
$\phi_{l,k,c,s}$	phase of the $c$ th cluster from the $k$ th antenna of transmitter to the $l$ th antenna of receiver via the $s$ th ray
$\psi_{c,s}^T$	azimuth angle of AoD (AAoD) from transmitter to $c$ th cluster via the $s$ th ray
$\theta_{c,s}^T$	elevation angle of AoD (EAoD) from transmitter to $c$ th cluster via the $s$ th ray
$\psi_{c,s}^R$	azimuth angle of AoA (AAoA) from $c$ th cluster to receiver via the $s$ th ray
$\theta_{c,s}^R$	elevation angle of AoA (EAoA) from $c$ th cluster to receiver via the $s$ th ray
$\alpha_{c,s}^T$	angle of AoD between $\mathbf{D}_{c,s}^T$ and $y$ axis from transmitter to $c$ th cluster via the $s$ th ray
$\alpha_{c,s}^R$	angle of AoA between $\mathbf{D}_{c,s}^R$ and $y$ axis from $c$ th cluster to receiver via the $s$ th ray

from the Tx to the  $c$ th cluster via the  $s$ th ray, while  $\alpha_{c,s}^R$  is the AoA between  $\mathbf{D}_{c,s}^R$  and  $y$  axis from the  $c$ th cluster to the Rx via the  $s$ th ray ( $s = 1, 2, \dots, S$ ). The multipath complex gains  $h_{l,k}(t, \tau)$  of the theoretical model ( $S \rightarrow \infty$ ) between  $\mathbf{A}_k^T$  and  $\mathbf{A}_l^R$  at delay  $\tau$  can be presented as

$$h_{l,k}(t, \tau) = \sum_{c=1}^N h_{l,k,c}(t) \delta(\tau - \tau_c) \quad (11)$$

where the complex gain  $h_{l,k,c}(t)$  of Cluster $_c$  can be computed

as

$$h_{l,k,c}(t) = \underbrace{\delta(c-1) \sqrt{\frac{K}{K+1}} e^{j(2\pi f_{l,k}^{\text{LOS}}(t)t + \phi_{l,k}^{\text{LOS}}(t))}}_{\text{LOS}} + \underbrace{\sqrt{\frac{P_c}{K+1}} \lim_{S \rightarrow \infty} \left( \frac{1}{\sqrt{S}} \sum_{s=1}^S e^{j(2\pi f_{l,k,c,s}(t)t + \phi_{l,k,c,s}(t))} \right)}_{\text{NLOS}}. \quad (12)$$

#### A. For the LOS component

The Doppler frequency of the  $l$ th receive antenna from the  $k$ th transmit antenna  $f_{l,k}^{\text{LOS}}(t)$  is expressed as

$$f_{l,k}^{\text{LOS}}(t) = f_{\max} \frac{\langle \mathbf{D}_{l,k}^{\text{LOS}}(t), \mathbf{v} - \mathbf{v}_c \rangle}{\|\mathbf{D}_{l,k}^{\text{LOS}}(t)\| \|\mathbf{v} - \mathbf{v}_c\|}. \quad (13)$$

The received phase of the  $l$ th receive antenna via the  $s$ th ray within the  $c$ th cluster from the  $k$ th transmit antenna can be expressed as

$$\phi_{l,k}^{\text{LOS}}(t) = \phi_0 + \frac{2\pi}{\lambda} \|\mathbf{D}_{l,k}^{\text{LOS}}(t)\| \quad (14)$$

where the distance between the  $l$ th receive antenna and the  $k$ th transmit antenna can be computed by the antenna vector  $\mathbf{A}_k^T(t)$ ,  $\mathbf{A}_l^R(t)$ , and the distance between the Tx and Rx along with the  $y$  axis  $\mathbf{D}$ , i.e.,

$$\mathbf{D}_{l,k}^{\text{LOS}}(t) = \mathbf{D}_{l,0}^{\text{LOS}}(t) - \mathbf{A}_k^T(t) \quad (15)$$

$$\mathbf{D}_{l,0}^{\text{LOS}}(t) = \mathbf{D} + \mathbf{A}_l^R(t) \quad (16)$$

#### B. For the NLOS component

The Doppler frequency of the Rx via the  $s$ th ray of the  $c$ th cluster  $f_{c,s}(t)$  can be expressed as

$$f_{c,s}(t) = f_{\max} \frac{\langle \mathbf{D}_{c,s}^R(t), \mathbf{v} - \mathbf{v}_c \rangle}{\|\mathbf{D}_{c,s}^R(t)\| \|\mathbf{v} - \mathbf{v}_c\|}. \quad (17)$$

Similar to the LOS component, the received phase of the Rx via the  $s$ th ray of the  $c$ th cluster  $f_{c,s}(t)$  can be computed as

$$\phi_{l,k,c,s}(t) = \phi_0 + \frac{2\pi}{\lambda} (\|\mathbf{D}_{l,c,s}^R(t)\| + \|\mathbf{D}_{k,c,s}^T(t)\|) \quad (18)$$

where the absolute distance between the Tx and Rx via the  $s$ th ray of the  $c$ th cluster can be derived according to their geometrical relationships:

$$\|\mathbf{D}_{c,s}^R(t)\| = \frac{2a_c \sin \alpha_{c,s}^T}{\sin \alpha_{c,s}^T + \sin(\pi - \alpha_{c,s}^R)}. \quad (19)$$

As a result, we can get the distance vector and the angle relationships:

$$\mathbf{D}_{c,s}^R(t) = \|\mathbf{D}_{c,s}^R(t)\| \begin{pmatrix} \cos \psi_{c,s}^R(t) \cos \theta_{c,s}^R(t) \\ \sin \psi_{c,s}^R(t) \cos \theta_{c,s}^R(t) \\ \sin \theta_{c,s}^R(t) \end{pmatrix}. \quad (20)$$

Based on the above equations, we can get

$$\mathbf{D}_{l,c,s}^R(t) = \mathbf{D}_{c,s}^R(t) - \mathbf{A}_l^R(t) \quad (21)$$

$$\mathbf{D}_{k,c,s}^T(t) = \mathbf{D}_{c,s}^T(t) - \mathbf{A}_k^T(t) \quad (22)$$

$$\mathbf{D}_{c,s}^T(t) = \mathbf{D} - \mathbf{D}_{c,s}^R(t) \quad (23)$$

$$\alpha_{c,s}^R = \arccos(\cos\theta_{c,s}^R \times \sin\psi_{c,s}^R). \quad (24)$$

For the NLOS components, AoAs  $\alpha_{c,s}^R$  and AoDs  $\alpha_{c,s}^T$  are dependent in an ellipsoid model. Their relationship can be expressed as [11]

$$\alpha_{c,s}^T = \begin{cases} g(\alpha_{c,s}^R) & \text{if } 0 < \alpha_{c,s}^R \leq \alpha_0 \\ g(\alpha_{c,s}^R) + \pi & \text{if } \alpha_0 < \alpha_{c,s}^R \leq 2\pi - \alpha_0 \\ g(\alpha_{c,s}^R) + 2\pi & \text{if } 2\pi - \alpha_0 < \alpha_{c,s}^R \leq 2\pi \end{cases} \quad (25)$$

$$g(\alpha_{c,s}^R) = \arctan\left(\frac{(k_0^2 - 1)\sin\alpha_{c,s}^R}{2k_0 + (k_0^2 + 1)\cos\alpha_{c,s}^R}\right) \quad (26)$$

$$\alpha_0 = \pi - \arctan\left(\frac{k_0^2 - 1}{2k_0}\right) \quad (27)$$

$$k_0 = \frac{a_c}{f}. \quad (28)$$

Given the semi-major axis  $f$  of the first ellipsoid,  $a_c$  can be determined by  $\tau_c(t)$  relative to the first ellipsoid as

$$a_c = w\tau_c(t) + a_1 \quad (29)$$

where  $w$  is the speed of light. The delay of the  $c$ th cluster is assumed to be the sum of two components, i.e.,

$$\tau_c(t) = \frac{\|\mathbf{D}_{c,s}^R(t)\| + \|\mathbf{D}_{c,s}^T(t)\|}{w} \quad (30)$$

### III. STATISTIC PROPERTIES

In this section, we will derive the corresponding statistical properties of wideband multi-confocal ellipsoid model.

#### A. Spatial-Temporal Correlation Function

The spatial-temporal correlation function between the channel gains  $h_{l,k,c}(t)$  and  $h_{l',k',c}(t)$  is defined as [9]

$$\rho_{lk,l'k',c}(\delta_T, \delta_R, \Delta t; t) = \mathbf{E} \left[ \frac{h_{l,k,c}^*(t)h_{l',k',c}(t + \Delta t)}{|h_{l,k,c}^*(t)||h_{l',k',c}(t + \Delta t)|} \right]. \quad (31)$$

When the LOS component and NLOS components are independent, it can be rewritten as

$$\begin{aligned} & \rho_{lk,l'k',c}(\delta_T, \delta_R, \Delta t; t) \\ &= \rho_{lk,l'k',c}^{\text{LOS}}(\delta_T, \delta_R, \Delta t; t) + \rho_{lk,l'k',c}^{\text{NLOS}}(\delta_T, \delta_R, \Delta t; t) \end{aligned} \quad (32)$$

where

$$\begin{aligned} \rho_{lk,l'k',c}^{\text{LOS}}(\delta_T, \delta_R, \Delta t; t) &= \frac{K\delta(c-1)}{K+1} \\ & e^{j[2\pi f_{l'k'}^{\text{LOS}}(t+\Delta t)(t+\Delta t) - 2\pi f_{lk}^{\text{LOS}}(t)(t) + \phi_{l'k'}^{\text{LOS}}(t+\Delta t) - \phi_{lk}^{\text{LOS}}(t)]} \end{aligned} \quad (33)$$

$$\begin{aligned} & \rho_{lk,l'k',c}^{\text{NLOS}}(\delta_T, \delta_R, \Delta t; t) \\ &= \frac{1}{K\delta(c-1) + 1} \mathbf{E} \left[ \lim_{S \rightarrow \infty} \left( \frac{1}{\sqrt{S}} \sum_{s=1}^S e^{j\Phi_0} \right) \right] \end{aligned} \quad (34)$$

with

$$\begin{aligned} \Phi_0 &= 2\pi f_{l',c,s}(t + \Delta t)(t + \Delta t) - 2\pi f_{l,c,s}(t)(t) \\ &+ \phi_{l'k',c,s}(t + \Delta t) - \phi_{lk,c,s}(t). \end{aligned} \quad (35)$$

#### B. Spatial Cross-Correlation Function

The spatial cross-correlation function (CCF)  $\rho_{lk,l'k',c}(\delta_T, \delta_R; t)$  can be obtained from the spatial-temporal correlation function by setting  $\Delta t = 0$ , i.e.,

$$\rho_{lk,l'k',c}(\delta_T, \delta_R; t) = \mathbf{E} \left[ \frac{h_{l,k,c}^*(t)h_{l',k',c}(t)}{|h_{l,k,c}^*(t)||h_{l',k',c}(t)|} \right]. \quad (36)$$

#### C. Temporal Auto-Correlation Function

By setting  $l = l'$  and  $k = k'$ , the spatial-temporal correlation function reduces to the temporal auto-correlation function (ACF)  $\rho_{lk,c}(\Delta t; t)$ , i.e.,

$$\rho_{lk,c}(\Delta t; t) = \mathbf{E} \left[ \frac{h_{l,k,c}^*(t)h_{l,k,c}(t + \Delta t)}{|h_{l,k,c}^*(t)||h_{l,k,c}(t + \Delta t)|} \right]. \quad (37)$$

## IV. SIMULATION MODEL

In the proposed theoretical channel model (reference model), the number of clusters is assumed to be infinity ( $S \rightarrow \infty$ ). However, with respect to a channel simulator, to compromise between accuracy and complexity, a finite number of clusters is practical. In this section, we will generate a channel simulator with a finite and proper cluster number when describing channel characteristics as accurately as possible. Thus, the simulation model of the proposed MIMO channel model is obtained as

$$\begin{aligned} h_{l,k,c}(t) &= \underbrace{\delta(c-1) \sqrt{\frac{K}{K+1}} e^{j(2\pi f_{l,k}^{\text{LOS}}(t)t + \phi_{l,k}^{\text{LOS}}(t))}}_{\text{LOS}} \\ &+ \underbrace{\sqrt{\frac{P_c}{K+1}} \left( \frac{1}{\sqrt{S}} \sum_{s=1}^S e^{j(2\pi f_{l,k,c,s}(t)t + \phi_{l,k,c,s}(t))} \right)}_{\text{NLOS}}. \end{aligned} \quad (38)$$

We define the spatial-temporal correlation function  $\rho_{lk,l'k',c}(\delta_T, \delta_R, \Delta t; t)$  with AoAs/AoDs distributed according to the cumulative distribution function (CDF) and we calculate it by the method of equal areas (MEA) in [9].

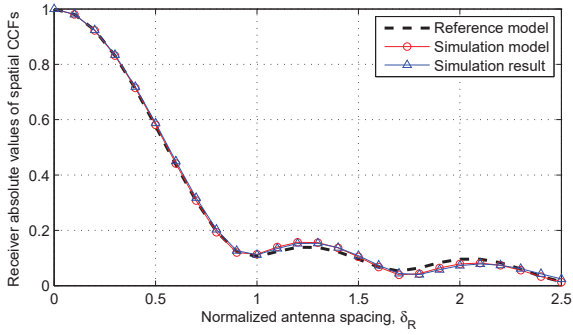


Fig. 3: The comparison of the spatial CCFs of the reference model, simulation model, and simulation result ( $M_T = 4, M_R = 4, l = 1, k = 1, l' = 2, k' = 1, D = 200$  m,  $\mathbf{v} = 10$  m/s,  $\lambda = 0.15$  m,  $\mathbf{v}_c = 1.5$  m/s).

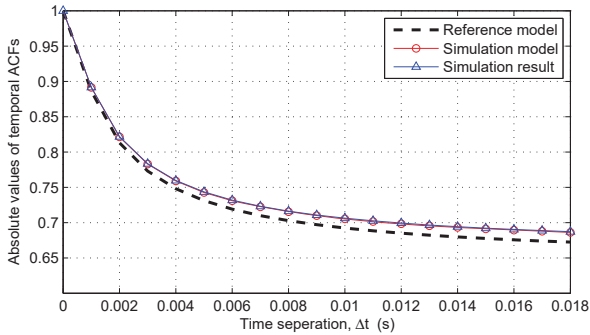


Fig. 4: The comparison of the temporal ACFs of the reference model, simulation model, and simulation result ( $M_T = 4, M_R = 4, D = 100$  m,  $\mathbf{v} = 30$  m/s,  $\lambda = 0.15$  m,  $\mathbf{v}_c = 3$  m/s).

## V. RESULTS AND DISCUSSIONS

Fig. 3 and Fig. 4 compare the spatial CCFs and temporal ACFs of the reference model, simulation model, and simulation results, respectively. All the results align well, clearly demonstrating that the derivations and simulations are valid.

Fig. 5 shows that the temporal ACF without time evolution is in general larger than that with time evolution. Therefore, it is necessary to consider a channel model with time evolution. In Fig. 6, we can see the difference between  $t = 1$  s and  $t = 4$  s in terms of temporal ACFs. So, the model is non-stationary.

In Fig. 7, we can see that the spatial CCF of the 3-D ellipsoid model is in general smaller than that of the 2-D ellipse model. The temporal ACF of the 3-D ellipsoid model is smaller than that of the 2-D ellipse model, as illustrated in Fig. 8. Hence, the 2-D ellipse model is not accurate, while the 3-D ellipsoid model gives more complete information.

## VI. CONCLUSIONS

In this paper, we have proposed a novel theoretical 3-D wideband multi-confocal ellipsoid channel model, along with its corresponding simulation model, for wireless MIMO

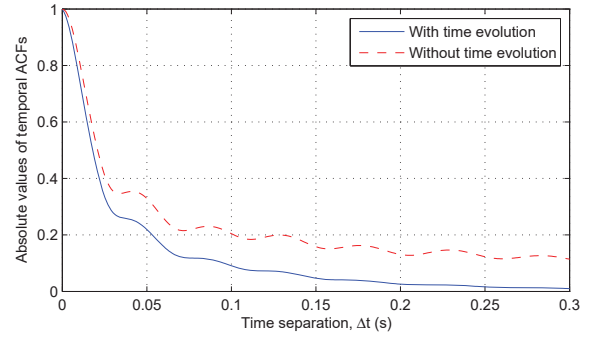


Fig. 5: The comparison of the temporal ACFs with and without time evolution ( $M_T = 8, M_R = 8, D = 100$  m,  $\mathbf{v} = 100$  m/s,  $\lambda = 0.15$  m,  $\mathbf{v}_c = 5$  m/s,  $T_0(\text{initial time}) = 1$  s).

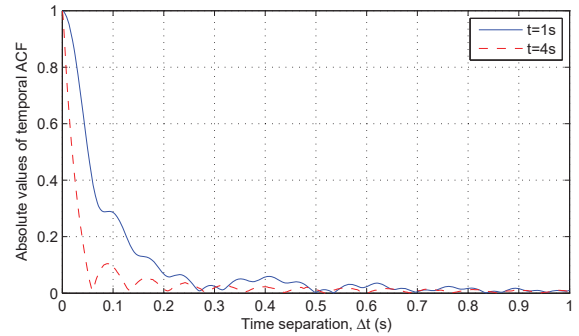


Fig. 6: The comparison of the temporal ACFs at different time instants ( $M_T = 8, M_R = 8, D = 300$  m,  $\mathbf{v} = 5$  m/s,  $\lambda = 0.15$  m,  $\mathbf{v}_c = 0.5$  m/s).

systems. The impact of elevation angles on the statistical properties of the MIMO channel model has been investigated. Most importantly, numerical and simulation results have verified that the channel characteristics of the simulation model can well align with those of the theoretical model. For future work, important parameters of the proposed MIMO channel model need to be better characterized via channel measurements. Also, the extension of the proposed model to support massive

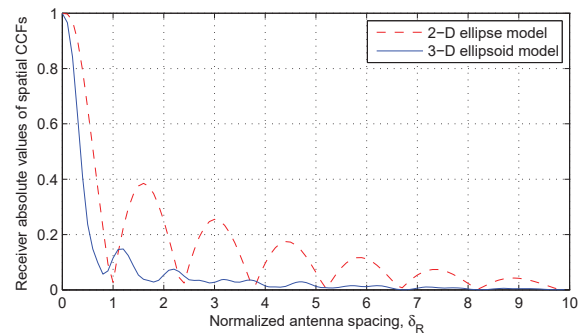


Fig. 7: The comparison of the spatial CCFs between the 2-D ellipse model and 3-D ellipsoid model ( $M_T = 8, M_R = 8, D = 300$  m,  $\mathbf{v} = 5$  m/s,  $\lambda = 0.15$  m,  $\mathbf{v}_c = 0.5$  m/s,  $T_0(\text{initial time}) = 4$  s).

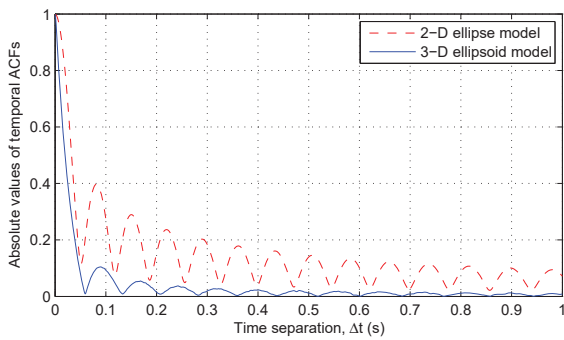


Fig. 8: The comparison of the temporal ACFs between the 2-D ellipse model and 3-D ellipsoid model ( $M_T = 8, M_R = 8, D = 300$  m,  $\mathbf{v} = 5$  m/s,  $\lambda = 0.15$  m,  $\mathbf{v}_c = 0.5$  m/s,  $T_0$  (initial time) = 4 s).

MIMO is another interesting research direction.

## VII. ACKNOWLEDGEMENT

This work was supported by the EU H2020 ITN 5G Wireless project (No. 641985), EU FP7 QUICK project (No. PIRSES-GA-2013-612652), National Natural Science Foundation of China (No. 61371110, 61231009), National Science and Technology Major Project (No. 2014ZX03003012-001), MOST 863 project in 5G (No. 2014AA01A707), and the Science and Technology Commission of Shanghai Municipality (STCSM) (No. 14DZ2290500).

## REFERENCES

- [1] X. Ge, H. Cheng, M. Guizani, T. Han, 5G wireless backhaul networks: challenges and research advances, *IEEE Network*, vol. 28, no. 6, pp. 6-11, Nov. 2014.
- [2] W. Weichselberger, M. Herdin, "A stochastic MIMO channel model with joint correlation of both link ends", *IEEE Trans. Wireless Commun.*, vol. 5, no. 1, pp. 90-100, Jan. 2006.
- [3] A. Sayeed, "Deconstructing multi-antenna fading channels", *IEEE Trans. Sig. Proc.*, vol. 50, no. 10, pp. 2563-2578, Oct. 2002.
- [4] J. Kermaol, L. Schumacher, and K. Pedersen "A stochastic MIMO radio channel model with experimental validation", *IEEE J. Sel. Areas Commun.*, vol. 20, no. 6, pp. 1211-1226, Aug. 2002.
- [5] X. Hong, C.-X. Wang, B. Allen, and W. Malik, "A correlation based double-directional stochastic channel model for multiple-antenna UWB systems," *IET Microwaves, Antennas & Propagation.*, vol. 1, no. 6, pp. 1182-1191, Dec. 2007.
- [6] C.-N. Chuah, D. N. C. Tse, J. M. Kahn, and R. A. Valenzuela, "Capacity scaling in MIMO wireless systems under correlated fading," *IEEE Trans. Inf. Theory*, vol. 48, no. 3, pp. 637-650, Mar. 2002.
- [7] G. Taricco, "Asymptotic mutual information statistics of separately correlated Rician fading MIMO channels," *IEEE Trans. Inf. Theory*, vol. 54, no. 8, pp. 3490-3504, Aug. 2008.
- [8] C.-K. Wen, S. Jin, and K.-K. Wong, "On the sum-rate of multiuser MIMO uplink channels with jointly-correlated Rician fading," *IEEE Trans. Commun.*, vol. 59, no. 10, pp. 2883-2895, Oct. 2011.
- [9] M. Patzold, *Mobile Radio Channels*, 2nd ed. West Sussex, U.K.: Wiley, 2012.
- [10] A. G. Zajic and G. L. Stuber, "Correlated mobile-to-mobile channels: modelling and simulation," *IEEE Trans. Veh. Technol.*, vol. 57, no. 2, pp. 715-726, Mar. 2008.
- [11] M. Patzold, B. O. Hogstad, and N. Youssef, "Analysis, and simulation of MIMO mobile-to-mobile fading channels," *IEEE Trans. Wireless Commun.*, vol. 7, no. 2, pp. 510-520, Feb. 2008.
- [12] A. Ghazal, C.-X. Wang, B. Ai, D. Yuan, and H. Haas, "Non-stationary wideband MIMO channel model for high-mobility intelligent transportation systems," *IEEE Trans. Intell. Transp. Syst.*, vol. 16, no. 2, pp. 885-897, Apr. 2015.
- [13] X. Cheng, C.-X. Wang, D. I. Laurenson, S. Salous, and A. V. Vasilakos, "An adaptive geometry-based stochastic model for non-isotropic MIMO mobile-to-mobile channels," *IEEE Trans. Wireless Commun.*, vol. 8, no. 9, Sep. 2009, pp. 4824-4835.
- [14] X. Cheng, C.-X. Wang, B. Ai, and H. Aggoune, "Level crossing rate and average fade duration of non-isotropic vehicle-to-vehicle Ricean fading channels," *IEEE Trans. Intell. Transp. Syst.*, vol. 15, no. 1, pp. 62-72, Feb. 2014.
- [15] Y. Yuan, C.-X. Wang, and X. Cheng "Novel 3D geometry-based stochastic models for non-isotropic MIMO vehicle-to-vehicle channels", *IEEE Trans. Wireless Commun.*, vol. 13, no. 1, pp. 298-309, Jan. 2014.
- [16] L. F. Liu, C. Oestges, J. Poutanen, The COST 2100 MIMO Channel Model, *IEEE Wireless Commun. Mag.*, vol. x, no. x, pp. 1536-1284, Dec. 2012
- [17] P. Kyösti, et al., "WINNER II channel models," IST-4-027756, WINNER II D1.1.2, v1.2, Apr. 2008.
- [18] ITU-R M.2135-1, "Guidelines for Evaluation of Radio Interface Technologies for IMT-Advanced," Geneva, Switzerland, Rep. ITU-R M.2135-1, Dec. 2009.
- [19] 3GPP T.R. 36.873, *Study on 3D channel model for LTE*, V2.0.0, 2014.
- [20] A. Paulraj, R. Nabar, and D. Gore, *Introduction to Space-Time Wireless Communications.*, Cambridge University Press, Cambridge, 2008.
- [21] T. Zwick, C. Fischer, D. Didascalou, and W. Wiesbeck, "A stochastic spatial channel model based on wave-propagation modeling," *IEEE J. Sel. Areas Commun.*, vol. 18, no. 1, pp. 6-15, Jan. 2000.